

## **Supplementary Information**

### Substrate-Selective Inhibitors that Reprogram the Activity of Insulin-Degrading Enzyme

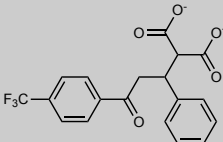
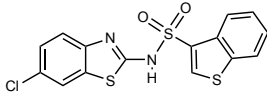
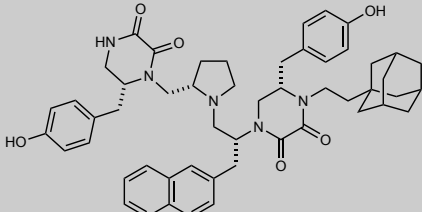
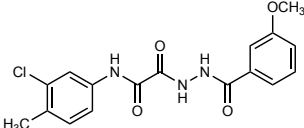
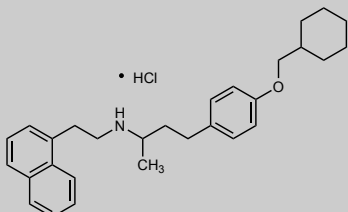
Juan Pablo Maianti, Grace A. Tan, Amedeo Vetere, Amie J. Welsh, Bridget K. Wagner, Markus A. Seeliger, and David R. Liu.

Correspondence: [drliu@fas.harvard.edu](mailto:drliu@fas.harvard.edu), [markus.seeliger@stonybrook.edu](mailto:markus.seeliger@stonybrook.edu)

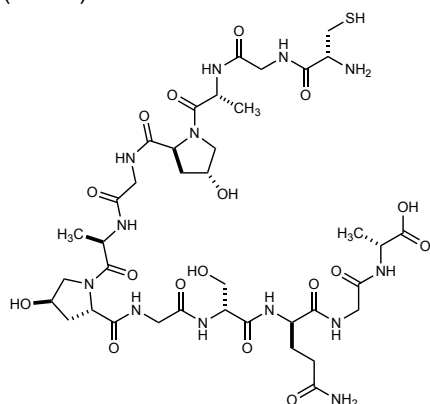
#### **This PDF includes:**

Supplementary Table 1 .....	2
Supplementary Table 2 .....	4
Supplementary Table 3 .....	5
Supplementary Table 4 .....	8
Supplementary Table 5 .....	9
Supplementary Table 6 .....	10
Supplementary Table 7 .....	11
Supplementary Table 8 .....	12
Supplementary Table 9 .....	13
Supplementary Figure 1 .....	14
Supplementary Figure 2 .....	16
Supplementary Figure 3 .....	18
Supplementary Figure 4 .....	20
Supplementary Figure 5 .....	22
Supplementary Figure 6 .....	24
Captions for Supplementary Data Sets .....	25
Supplementary References .....	26

**Supplementary Table 1.** Substrate-discriminating exo-site ligands previously reported.<sup>a</sup>

Enzyme, ligand structure, exo site	Potency, ligand properties	Substrate-discrimination observations	Suppl. Ref.
<p>Phosphoinositide-dependent kinase-1 (PDK1)</p>  <p>Name: "PS210" (and diester "PS423") Allosteric PIF-binding pocket</p>	<p><math>AC_{50} = 2 \mu M</math></p> <p>A diester was used to promote cell penetration</p> <p><math>EC_{50}</math> of other substrates n.d.</p>	<p>Activator of kinase activity ~10-fold in an <i>in vitro</i> peptide phosphorylation assay. In cell-based assays treatment with the diester analog PS423 inhibited S6K phosphorylation but not Akt phosphorylation. Substrate-discrimination is explained through PDK1-Akt interactions that are strongly promoted through their co-localization to the cell membrane.</p>	1,2
<p>Phosphoinositide-dependent kinase-1 (PDK1)</p>  <p>Name: "RS1" Allosteric PIF-binding pocket</p>	<p><math>K_d = 1.5 \mu M</math></p> <p><math>EC_{50}</math> of other substrates n.d.</p>	<p>Activator of kinase activity ~2-fold in an <i>in vitro</i> peptide phosphorylation assay, and inhibited 75% S6K phosphorylation <i>in vitro</i>. In cell-based assays RS1 inhibited S6K phosphorylation (by 50% vs a control ATP-competitive PDK1 inhibitor) but not Akt phosphorylation. Substrate-discrimination is explained through PDK1-Akt interactions that are strongly promoted through their co-localization to the cell membrane.</p>	2,3
<p>A disintegrin and metalloprotease 17 (ADAM17)</p>  <p>Name: "ligand 17" Unknown binding site (n.d.)</p>	<p><math>IC_{50} = 4.2 \mu M</math> (TNF<math>\alpha</math>-based glycosylated substrate cleavage)</p> <p><math>EC_{50}</math>'s for other substrates n.d.</p>	<p>Cell culture assays showed inhibition of shedding of Heregulin (100%), PTK7 (50–82%), TNF<math>\alpha</math> (43%), IL-8 (36%) but no inhibition of shedding of betacellulin or TGF<math>\alpha</math> (0%).</p>	4
<p>A disintegrin and metalloprotease 10 (ADAM10)</p>  <p>Name: "CID 31176944" Unknown binding site (n.d.)</p>	<p><math>IC_{50} = 1.1 \mu M</math> (glycosylated peptide cleavage, est. <math>K_i = 0.88 \mu M</math>)</p> <p><math>EC_{50}</math> of other substrates n.d.</p>	<p>Inhibitor of <i>in vitro</i> cleavage of a glycosylated peptide, but not the unmodified peptide. Cell culture assays showed inhibition of HER2 and CXCL16 shedding, but not syndecan-4 shedding inhibition.</p>	5
<p>Thrombin</p>  <p>Name: "LY254603" Unknown binding site (n.d.)</p>	<p><math>IC_{50} = 3 \mu M</math> (fibrinogen assay) <math>AC_{50} = 3 \mu M</math> (protein-C assay)</p>	<p>Inhibitor of fibrinogen cleavage, and activator of protein-C by up to 10-fold. Potentially mimics the thrombomodulin allosteric mechanism on thrombin.</p>	6

Matrix metalloproteinase-2  
(MMP2)



$IC_{50} = 30 \mu M$   
(gelatin cleavage)

The ligand corresponds to human collagen  $\alpha 1(I)$  residues 715-721: CGAOGAOGSQA, where "O" is 4-hydroxyproline

Inhibitor of gelatin cleavage by 90%, but a minimal inhibitor of cleavage of the fluorogenic substrate NFF-1.

7

Name "peptide P713"  
Collagen-binding domain (CBD)

Matrix metalloproteinase-9 and -2  
(MMP9 and MMP2)

$K_i \approx 50 \mu M$   
(gelatin cleavage)

Triple helical peptide (GPO)<sub>4</sub>-GAOG-AOGSQAOG-(GPO)<sub>3</sub>-GPY-NH<sub>2</sub>

The ligand is a triple-helical peptide based on the human collagen  $\alpha 1(I)$  residues 715-721 (see P713 above).

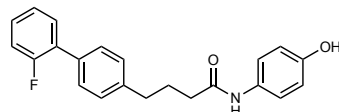
Inhibitor of MMP9- and MMP2-mediated gelatin cleavage ( $K_i \approx 50 \mu M$ ) and  $\alpha 1(V)$  436-447 fTHP cleavage ( $K_i \approx 120-140 \mu M$ ), but not an inhibitor of cleavage of small fluorogenic peptide substrates.

8

where "O" is 4-hydroxyproline

Name " $\alpha 1(I)$ 715-721 THP"  
Collagen-binding domain (CBD)

MAPK14/P38 $\alpha$



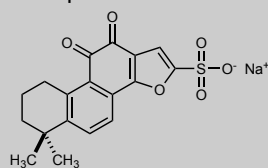
$K_d = 1 \mu M$  (ITC)  
( $K_i$  and  $IC_{50}$  reports vary)

Inhibitor of p38 $\alpha$ -mediated activation of MK2-a isoform in an *in vitro* assay, but not in ATF2 phosphorylation ( $>20 \mu M$ ). The substrate selective mechanism may be explained by an uncompetitive mechanism that blocks p38 $\alpha$  in the presence of MK2a by stabilizing the p38 $\alpha$ -MK2a interaction.

9,10

Name "CMPD1"  
Unknown binding site (n.d.)

Cathepsin K



$IC_{50} = 2.7 \mu M$   
(soluble collagen)

Inhibitor of soluble, insoluble, and fibrillar collagen degradation but did not inhibit gelatin degradation (0%, at 12.5  $\mu M$  concentration) nor inhibited the cleavage of fluorogenic substrate Cbz-Phe-Arg-Mca.

11,12

Name "TC06"  
Glycosaminoglycan binding site

<sup>a</sup> Not included in this summary: 1) active-site-targeted COX2 inhibitors that act through a homodimer allosteric mechanism effecting changes on the inhibitor  $K_i$  and substrate affinity of the active site of the neighboring subunit<sup>13</sup>; 2) gamma-secretase inhibitors that preferentially inhibit presenilin isoform PS1 over isoform PS2, which comprise the two possible catalytic cores of gamma-secretase complexes<sup>14</sup>; and 3) APP cleavage inhibitors that bind the substrate rather than the BACE enzyme<sup>15,16</sup>.

**Supplementary Table 2.** Screening strategy for identifying IDE exo-site ligands.

Category	Parameter	Description
<b>Assay</b>	Type of assay	Fluorescence anisotropy probe displacement assay ( $Z' > 0.7$ )
	Target	Recombinant human Insulin-Degrading Enzyme (main isoform, full length, wildtype)
	Primary measurement	Fluorescence anisotropy (excitation 492 nm, emission 523 nm)
	Key reagents	FL-6b ( <b>4</b> ) anisotropy probe and His <sub>6</sub> -IDE
	Assay protocol	See full description in Online Methods
<b>Library</b>	Library size	17,277 total compounds tested in two screens: 9,597 "DOS Informer Set" compound collection of 25 selected plates representative of small-molecule libraries at the Broad Institute; and additional 7,679 azetidine-core sub-library compounds <sup>17</sup> .
	Library composition	Diversity-oriented synthesis library collection at the Broad Institute and azetidine-core sub-libraries <sup>17</sup> .
	Source	Broad Institute
<b>Screen</b>	Format	384 well plates
	Concentrations(s) tested	20 $\mu$ M (0.2% v/v DMSO)
	Plate controls	Negative control, DMSO (0.2% v/v); Positive control, 20 $\mu$ M 6bK ( <b>1</b> ) inhibitor <sup>18</sup> .
	Reagent/compound dispensing system	IDE and FL-6b ( <b>4</b> ) probe were dispensed by a Multidrop Combi-nL Reagent Dispenser (Thermo Scientific). For the pilot screen a CyBio Vario CyBio Vario liquid handling system equipped with a pin-transfer workstation, and a liquid handling system equipped with a pin-transfer workstation was used. For the second screen of azetidine-core libraries the compounds were pre-loaded in empty 384-well plates by sonication using an Echo 555 Liquid Handler (Labcyte) and the enzyme-probe mixture was dispensed to the plate. See Online Methods and PubChem BioAssay database #1259349.
	Detection instrument and software	EnVision spectrophotometer and software (Perkin Elmer)
	Assay validation/QC	$Z' = 0.7$
	Correction factors	None
	Normalization	Z-factor normalization was calculated using the negative control signals in each plate. Raw data is available in PubChem BioAssay database #1259349.

<b>Post-HTS analysis</b>	Hit criteria	Z-factor < -12.5 average for both replicates
	Hit rate	0.35% for the unbiased "DOS Informer Set" pilot screen, and 1.3% for the azetidine sub-library <sup>17</sup> . See main text for discussion.
	Additional assay(s)	Hits were counter-screened for functional inhibition of IDE-mediated cleavage of the substrate Mca-RPPGFSAFK(Dnp)-OH (R&D Systems, #ES005) using high-purity, commercially available recombinant human IDE (R&D Systems #2496-ZN). This data is available in PubChem BioAssay database #1259348.
	Confirmation of hit purity and structure	Re-synthesis of hit BRD8283 ( <b>5</b> ), <sup>1</sup> H- and <sup>13</sup> C-NMR, Mosher ester diastereomeric purity, absolute stereochemical assignment by X-ray crystallography of intermediate <b>66</b> . Formula confirmation by high-resolution mass spectrometry was obtained for all library hits and analogs.

### Supplementary Table 3.

IDE inhibition EC<sub>50</sub> and percent inhibition maximum (I<sub>MAX</sub>) for azetidine analogs shown in Fig. 2A–C determined using the fluorogenic decapeptide reporter assay (Mca-RPPGFSAFK(Dnp)-OH)<sup>18,19</sup>. See also the counter-screen data for hit compounds identified in the Broad Institute library screens in PubMed BioAssay database 1259348. Purity and high-resolution mass spectrometry formula confirmation was performed by Harvard University Bauer Core and the Broad Institute Compound Management.

ID	Formula	SMILES code structure	EC <sub>50</sub> <sup>fluo</sup> ( $\mu$ M)	I <sub>MAX</sub> <sup>fluo</sup>	Calculated [M+H] <sup>+</sup>	Found [M+H] <sup>+</sup>	$\Delta$ (ppm)
FL-6b (4)	C <sub>67</sub> H <sub>74</sub> N <sub>8</sub> O <sub>16</sub>	<chem>O=C1OC2(c3c(Oc4c2ccc(O)c4)cc(O)cc3)c5c cc(cc15)C(NCCOCCOCCNC([C@H](CCCCN C([C@@H](Cc6ccc(C(c7ccccc7)=O)cc6)NC([ C@H](CC8CCCCC8)NC([C@H](CCC(N)=O) NC(/C=C/9)=O)=O)=O)NC9=O)=O)=O</chem>	0.1	100%	1247.5296	1247.5278	-1.4
6b- PEG- NH <sub>2</sub>	C <sub>46</sub> H <sub>64</sub> N <sub>8</sub> O <sub>10</sub>	<chem>O=C([C@@H](Cc1ccc(C(c2ccccc2)=O)cc1) NC([C@H](CC3CCCCC3)NC([C@H](CCC(N )=O)NC(/C=C/4)=O)=O)=O)NCCC[C@H] (C(NCCOCCOCCN)=O)NC4=O</chem>	0.05	100%	889.4818	889.4811	-0.88
21	C <sub>28</sub> H <sub>32</sub> N <sub>2</sub> O <sub>3</sub> S	<chem>OC[C@@H](N1CCCC(S(=O)(c2c(C)cccc2) =O)C[C@@H]31)[C@H]3c4ccc(c5ccccc5)cc 4</chem>	0.41	66%	477.2206	477.2202	-0.9
22	C <sub>29</sub> H <sub>34</sub> N <sub>2</sub> O <sub>4</sub> S	<chem>OC[C@@H](N1CCCC(S(=O)(c2c(C)cccc2) =O)C[C@@H]31)[C@H]3c4ccc(c5cc(OC)ccc 5)cc4</chem>	0.49	67%	507.2312	507.2307	-1.0
23	C <sub>30</sub> H <sub>36</sub> N <sub>2</sub> O <sub>3</sub> S	<chem>OC[C@@H](N1CCCC(S(=O)(c2c(C)cccc2) =O)C[C@@H]31)[C@H]3c4ccc(c5cc(C)c(C)c c5)cc4</chem>	0.14	55%	505.2519	505.2514	-1.1
24	C <sub>29</sub> H <sub>32</sub> N <sub>2</sub> O <sub>5</sub> S	<chem>OC[C@@H](N1CCCC(S(=O)(c2c(C)cccc2) =O)C[C@@H]31)[C@H]3c4ccc(c5cc6c(OCO 6)cc5)cc4</chem>	2.9	100%	521.2105	521.2098	-1.2
25	C <sub>28</sub> H <sub>32</sub> N <sub>2</sub> O <sub>4</sub> S	<chem>OC[C@@H](N1CCCC(S(=O)(c2c(C)cccc2) =O)C[C@@H]31)[C@H]3c4ccc(c5cc(OC)ccc5 )cc4</chem>	7.3	100%	493.2156	493.2113	-8.72
26	C <sub>29</sub> H <sub>34</sub> N <sub>2</sub> O <sub>3</sub> S	<chem>OC[C@@H](N1CCCC(S(=O)(c2c(C)cccc2) =O)C[C@@H]31)[C@H]3c4ccc(c5ccccc5C)c c4</chem>	0.032	63%	491.2363	491.2359	-0.7
27	C <sub>29</sub> H <sub>34</sub> N <sub>2</sub> O <sub>4</sub> S	<chem>OC[C@@H](N1CCCC(S(=O)(c2c(C)cccc2) =O)C[C@@H]31)[C@H]3c4ccc(c5ccccc5OC )cc4</chem>	0.25	68%	507.2312	507.2343	6.11
28	C <sub>30</sub> H <sub>36</sub> N <sub>2</sub> O <sub>3</sub> S	<chem>OC[C@@H](N1CCCC(S(=O)(c2c(C)cccc2) =O)C[C@@H]31)[C@H]3c4ccc(c5cc(C)cc(C) c5)cc4</chem>	0.061	75%	505.2519	505.2516	-0.6
29	C <sub>30</sub> H <sub>36</sub> N <sub>2</sub> O <sub>3</sub> S	<chem>OC[C@@H](N1CCCC(S(=O)(c2c(C)cccc2) =O)C[C@@H]31)[C@H]3c4ccc(c5cc(C)ccc5 C)cc4</chem>	0.054	64%	505.2519	505.2516	-0.6
30	C <sub>30</sub> H <sub>36</sub> N <sub>2</sub> O <sub>3</sub> S	<chem>OC[C@@H](N1CCCC(S(=O)(c2c(C)cccc2) =O)C[C@@H]31)[C@H]3c4ccc(c5c(C)c(C)cc c5)cc4</chem>	0.0015	59%	505.2519	505.2515	-0.9
31	C <sub>28</sub> H <sub>31</sub> FN <sub>2</sub> O <sub>3</sub> S	<chem>OC[C@@H](N1CCCC(S(=O)(c2c(C)cccc2) =O)C[C@@H]31)[C@H]3c4ccc(c5cc(F)ccc5) cc4</chem>	1.2	100%	495.2112	495.2109	-0.6
32	C <sub>29</sub> H <sub>30</sub> F <sub>4</sub> N <sub>2</sub> O <sub>3</sub> S	<chem>OC[C@@H](N1CCCC(S(=O)(c2c(C)cccc2) =O)C[C@@H]31)[C@H]3c4ccc(c5c(C(F)F)F )c(F)ccc5)cc4</chem>	0.17	54%	563.1986	563.1984	-0.4
33	C <sub>29</sub> H <sub>33</sub> FN <sub>2</sub> O <sub>3</sub> S	<chem>OC[C@@H](N1CCCC(S(=O)(c2c(C)cccc2) =O)C[C@@H]31)[C@H]3c4ccc(c5c(C)cc(F)cc c5)cc4</chem>	0.07	66%	509.2269	509.2266	-0.6
34	C <sub>30</sub> H <sub>30</sub> F <sub>6</sub> N <sub>2</sub> O <sub>3</sub> S	<chem>OC[C@@H](N1CCCC(S(=O)(c2c(C(F)F)F )cccc2)=O)C[C@@H]31)[C@H]3c4ccc(c5c(C )c(C(F)F)F)ccc5)cc4</chem>	0.095	68%	613.1954	613.1948	-1.0
35	C <sub>29</sub> H <sub>31</sub> ClN <sub>2</sub> O <sub>3</sub> S	<chem>OC[C@@H](N1C/C=C\N(S(=O)(c2c(C)ccc c2)=O)C[C@@H]31)[C@H]3c4ccc(c5c(C)c( Cl)ccc5)cc4</chem>	0.035	68%	523.1817	523.1814	-0.5
36	C <sub>28</sub> H <sub>25</sub> Cl <sub>2</sub> F <sub>3</sub> N <sub>2</sub> O <sub>3</sub> S	<chem>OC[C@@H](N1C/C=C\N(S(=O)(c2c(C(F)F )F)cccc2)=O)C[C@@H]31)[C@H]3c4ccc(c5c (Cl)c(Cl)ccc5)cc4</chem>	0.009	75%	597.0988	597.0983	-0.8
37	C <sub>30</sub> H <sub>33</sub> F <sub>3</sub> N <sub>2</sub> O <sub>3</sub> S	<chem>OC[C@@H](N1CCCC(S(=O)(c2c(C(F)F)F )cccc2)=O)C[C@@H]31)[C@H]3c4ccc(c5c( C)c(C)ccc5)cc4</chem>	0.001	70%	559.2237	559.223	-1.3

38	C <sub>30</sub> H <sub>32</sub> F <sub>4</sub> N <sub>2</sub> O <sub>2</sub> S	FC[C@@H](N1CCCCN(S(=O)(c2c(C(F)(F)F)cccc2)=O)C[C@@H]31)[C@H]3c4ccc(c5c(C)C)ccc5)cc4	0.024	46%	561.2193	561.2186	-1.1
39	C <sub>31</sub> H <sub>36</sub> F <sub>3</sub> N <sub>3</sub> O <sub>2</sub> S	O=S(N(C[C@@H]12)CCCCN2[C@H](CNC)[C@H]1c3ccc(c4c(C)C)ccc4)cc3)(c5c(C(F)(F)F)cccc5)=O	0.007	100%	572.2553	572.2548	-1.0
40	C <sub>32</sub> H <sub>38</sub> F <sub>3</sub> N <sub>3</sub> O <sub>2</sub> S	O=S(N(C[C@@H]12)CCCCN2[C@H](CN(C)C)[C@H]1c3ccc(c4c(C)C)ccc4)cc3)(c5c(C(F)(F)F)cccc5)=O	0.1	100%	586.271	586.2704	-1.0
41	C <sub>31</sub> H <sub>35</sub> F <sub>3</sub> N <sub>2</sub> O <sub>3</sub> S	O=S(N(C[C@@H]12)CCCCN2[C@H](COC)[C@H]1c3ccc(c4c(C)C)ccc4)cc3)(c5c(C(F)(F)F)cccc5)=O	0.075	100%	573.2393	573.2388	-0.9
42	C <sub>30</sub> H <sub>31</sub> F <sub>3</sub> N <sub>2</sub> O <sub>4</sub> S	OC([C@@H](N1CCCCN(S(=O)(c2c(C(F)(F)F)cccc2)=O)C[C@@H]31)[C@H]3c4ccc(c5c(C)C)ccc5)cc4)=O	0.5	100%	573.2029	573.2021	-1.4
43	C <sub>26</sub> H <sub>27</sub> F <sub>3</sub> N <sub>2</sub> O <sub>3</sub> S	OC[C@@H](N[C@H]1CNS(=O)(c2cccc2C(F)(F)F)=O)[C@H]1c3ccc(c4c(C)C)ccc4)cc3	0.59	85%	505.1767	505.1762	-1.1
44	C <sub>29</sub> H <sub>31</sub> F <sub>3</sub> N <sub>2</sub> O <sub>3</sub> S	OC[C@@H](N1CC=C)[C@H]1(C[C@@H]1CNS(=O)(c2cccc2C(F)(F)F)=O)c3ccc(c4cccc(C)c4C)cc3	0.1	90%	545.208	545.2076	-0.8
45	C <sub>28</sub> H <sub>29</sub> F <sub>3</sub> N <sub>2</sub> O <sub>4</sub> S	OC[C@@H](N1C(C)=O)[C@H]1(C[C@@H]1CNS(=O)(c2cccc2C(F)(F)F)=O)c3ccc(c4c(C)C)ccc4)cc3	0.115	86%	547.2737	547.2729	-1.5
46	C <sub>29</sub> H <sub>29</sub> F <sub>3</sub> N <sub>2</sub> O <sub>4</sub> S	OC[C@@H](N1C(CCN(S(=O)(c2cccc2C(F)(F)F)=O)C[C@@H]31)=O)[C@H]3c4ccc(c5c(C)C)ccc5)cc4	0.12	72%	559.1873	559.1865	-1.4
47	C <sub>30</sub> H <sub>31</sub> F <sub>3</sub> N <sub>2</sub> O <sub>4</sub> S	OC[C@@H](N1C(CCCN(S(=O)(c2cccc2C(F)(F)F)=O)C[C@@H]31)=O)[C@H]3c4ccc(c5c(C)C)ccc5)cc4	0.08	71%	573.2029	573.2021	-1.4
48	C <sub>31</sub> H <sub>33</sub> F <sub>3</sub> N <sub>2</sub> O <sub>4</sub> S	OC[C@@H](N(C(CCCC1)=O)[C@H]2CN1S(=O)(c3cccc3C(F)(F)F)=O)[C@H]2c4ccc(c5c(C)C)ccc5)cc4	0.1	87%	587.2186	587.2178	-1.4
49	C <sub>32</sub> H <sub>35</sub> F <sub>3</sub> N <sub>2</sub> O <sub>4</sub> S	OC[C@@H](N1[C@H]2CN(CCCC1)=O)S(=O)(c3cccc3C(F)(F)F)=O)[C@H]2c4ccc(c5c(C)ccc5)cc4	0.06	88%	601.2342	601.2335	-1.1
50	C <sub>29</sub> H <sub>40</sub> N <sub>2</sub> O <sub>3</sub> S	O=S(C1CCCC1)(N(C[C@@H]23)CCCCN3[C@H](CO)[C@H]2c4ccc(c5c(C)C)ccc5)cc4)=O	0.46	100%	497.2832	497.2828	-0.9
51	C <sub>29</sub> H <sub>33</sub> N <sub>3</sub> O <sub>3</sub> S	O=S(c1ccnc1C)(N(C[C@@H]23)C/C=C\N3[C@H](CO)[C@H]2c4ccc(c5c(C)C)ccc5)cc4)=O	0.022	41%	504.2315	504.2312	-0.7
52	C <sub>32</sub> H <sub>39</sub> N <sub>3</sub> O <sub>4</sub> S	O=S(c1ccc(NC(C)=O)cc1C)(N(C[C@@H]23)CCCCN3[C@H](CO)[C@H]2c4ccc(c5c(C)C)ccc5)cc4)=O	1.6	100%	562.2734	562.2729	-0.9
53	C <sub>29</sub> H <sub>38</sub> N <sub>4</sub> O <sub>3</sub> S	O=S(c1cnn1C(C)C)(N(C[C@@H]23)CCCCN3[C@H](CO)[C@H]2c4ccc(c5c(C)C)ccc5)cc4)=O	0.015	77%	523.2737	523.2732	-1.0
54	C <sub>29</sub> H <sub>36</sub> N <sub>4</sub> O <sub>3</sub> S	O=S(c1cnn1CCC)(N(C[C@@H]23)C/C=C\N3[C@H](CO)[C@H]2c4ccc(c5c(C)C)ccc5)cc4)=O	0.018	67%	521.2581	521.2578	-0.6
55	C <sub>28</sub> H <sub>34</sub> N <sub>4</sub> O <sub>3</sub> S	O=S(c1cnc(C)n1C)(N(C[C@@H]23)C/C=C\N3[C@H](CO)[C@H]2c4ccc(c5c(C)C)ccc5)cc4)=O	0.001	57%	507.2424	507.242	-0.8
56	C <sub>31</sub> H <sub>38</sub> N <sub>4</sub> O <sub>3</sub> S	O=S(c1cnc2n1CCCC2)(N(C[C@@H]34)C/C=C\N4[C@H](CO)[C@H]3c5ccc(c6c(C)C)ccc6)cc5)=O	0.042	45%	547.2737	547.2733	-0.7
57	C <sub>30</sub> H <sub>37</sub> N <sub>3</sub> O <sub>5</sub> S	O=S(c1n(C)C(C(OC)=O)cc1)(N(C[C@@H]23)CCCCN3[C@H](CO)[C@H]2c4ccc(c5c(C)C)ccc5)cc4)=O	>5	n/a	552.2527	552.2523	-0.7
58	C <sub>29</sub> H <sub>36</sub> N <sub>4</sub> O <sub>3</sub> S	O=S(c1cnn(C)C1C)(N(C[C@@H]23)C/C=C\N3[C@H](CO)[C@H]2c4ccc(c5c(C)C)ccc5)cc4)=O	0.016	53%	521.2581	521.2574	-1.3
59	C <sub>28</sub> H <sub>31</sub> F <sub>3</sub> N <sub>4</sub> O <sub>3</sub> S	O=S(c1cn(C)nc1C(F)(F)F)(N(C[C@@H]23)C/C=C\N3[C@H](CO)[C@H]2c4ccc(c5c(C)C)ccc5)cc4)=O	0.065	76%	561.2142	561.2133	-1.6
60	C <sub>28</sub> H <sub>40</sub> N <sub>4</sub> O <sub>3</sub> S	O=S(N1CCN(C)CC1)(N(C[C@@H]23)CCCCN3[C@H](CO)[C@H]2c4ccc(c5c(C)C)ccc5)cc4)=O	0.032	84%	513.2894	513.2895	-0.2
61	C <sub>28</sub> H <sub>36</sub> N <sub>4</sub> O <sub>3</sub> S	O=S(c1cc(C)nn1C)(N(C[C@@H]23)CCCCN3[C@H](CO)[C@H]2c4ccc(c5c(C)C)ccc5)cc4)=O	0.024	67%	509.2581	509.2577	-0.8
62	C <sub>27</sub> H <sub>34</sub> N <sub>4</sub> O <sub>3</sub> S	O=S(c1cnn1C)(N(C[C@@H]23)CCCCN3[C@H](CO)[C@H]2c4ccc(c5c(C)C)ccc5)cc4)=O	0.06	100%	495.2424	495.2419	-1.0
63	C <sub>27</sub> H <sub>34</sub> N <sub>4</sub> O <sub>3</sub> S	O=S(c1nccn1C)(N(C[C@@H]23)CCCCN3[C@H](CO)[C@H]2c4ccc(c5c(C)C)ccc5)cc4)=O	0.0005	60%	495.2424	495.2421	-0.7

### Supplementary Table 4.

Approximate calculation of the competitive inhibitor dissociation constant  $K_i^{\text{comp}} = IC_{50} / ([S]/K_M + 1)$  using the insulin assay potency ( $EC_{50}^{\text{ins}}$ ) for the inhibitors that satisfy the assumption of a competitive mode of inhibition by displaying complete blockage of IDE-mediated insulin degradation. A  $K_M$  value of 20 nM was used for the calculation; however, reports of insulin  $K_M$  for IDE vary from 10 to 65 nM<sup>20-22</sup>.

ID	Formula	SMILES code structure	$EC_{50}^{\text{fluo}}$ ( $\mu\text{M}$ )	$EC_{50}^{\text{ins}}$ ( $\mu\text{M}$ )	$K_i^{\text{comp}}$ ( $\mu\text{M}$ )
<b>6bK (1)</b>	$\text{C}_{67}\text{H}_{74}\text{N}_8\text{O}_{16}$	<chem>O=C1OC2(c3c(Oc4c2ccc(O)c4)cc(O)cc3)c5ccc(cc15)C(NCCOCCOCCNC([C@H](CCCCNC([C@@H](Cc6ccc(C(c7ccccc7)=O)cc6)NC([C@H](CC8CC8)NC([C@H](CCC(N)=O)NC(/C=C/9)=O)=O)=O)=O)NC9=O)=O)</chem>	0.050	0.150	0.128
<b>BRD8283 (5)</b>	$\text{C}_{30}\text{H}_{36}\text{N}_2\text{O}_3\text{S}$	<chem>Cc1cccc(c1)-c1ccc(cc1)[C@@H]1[C@@H](CO)N2CCCCN(C[C@@H]12)S(=O)(=O)c1cccc1C</chem>	0.100	0.190	0.162
<b>30</b>	$\text{C}_{30}\text{H}_{36}\text{N}_2\text{O}_3\text{S}$	<chem>OC[C@@H](N1CCCCN(S(=O)(c2c(C)ccc2)=O)C[C@@H]31)[C@H]3c4cc(c(c5c(C)c(C)ccc5)cc4</chem>	0.0015	0.007	0.006
<b>37</b>	$\text{C}_{30}\text{H}_{33}\text{F}_3\text{N}_2\text{O}_3\text{S}$	<chem>OC[C@@H](N1CCCCN(S(=O)(c2c(C(F)F)ccc2)=O)C[C@@H]31)[C@H]3c4ccc(c5c(C)c(C)ccc5)cc4</chem>	0.001	0.005	0.0043
<b>63</b>	$\text{C}_{27}\text{H}_{34}\text{N}_4\text{O}_3\text{S}$	<chem>O=S(c1ncn1C)(N(C[C@@H]23)CCCCN3[C@H](CO)[C@H]2c4ccc(c5c(C)c(C)ccc5)cc4)=O</chem>	0.0005	0.002	0.0017



**Supplementary Table 5.**

Summary of reagents and buffer conditions used in metalloprotease cleavage activity assays using fluorogenic peptide substrates in the presence of inhibitors.

Enzyme	Vendor, catalog	[E] final	Buffer, conditions	Substrate, source, and catalog/ref.	[S] ( $\mu$ M)	Time (min)	Ex (nm)	Em (nm)
IDE	R&D #2496-ZN	85 ng/mL	50 mM Tris pH 7.5, 1 M NaCl, 23 °C	Subtrate V, R&D, #ES005	10	5	320	405
NEP	R&D #1182-ZNC	50 ng/mL	50 mM Tris pH 9, 0.05% Birj, 23 °C	Subtrate V, R&D, #ES005	10	5	320	405
ACE	R&D #929-ZN	200 ng/mL	50 mM MES pH 6.5, 23 °C	Subtrate V, R&D, #ES005	10	5	320	405
THOP	R&D #3439-ZN	250 ng/mL	25 mM Tris pH 8, 150 mM NaCl, 23 °C	Mca-PLGPK(Dnp)-OH, Bachem, #M-2710	10	5	320	405
NLN	R&D #3814-ZN	1 $\mu$ g/mL	25 mM Tris pH 7.5, 150 mM NaCl, 23 °C	Mca-PLGPK(Dnp)-OH, Bachem, #M-2710	25	5	320	405
MMP1*	R&D #901-MP	500 ng/mL	50 mM Tris pH 7.5, 10 mM CaCl <sub>2</sub> , 0.05% Birj, 23 °C	Mca-PLGL-Dpa-AR-NH <sub>2</sub> , R&D, #ES001	10	5	320	405
NRDC	LSBio, LS-G70915	20 $\mu$ g/mL	1 $\mu$ M ZnCl <sub>2</sub> , 30 mM Tris, pH 7.5, 10 mM KCl, 5 mM MgCl <sub>2</sub> and 1 mM DTT <sup>23</sup> , 28 °C	Abz-GGFHRRHGQ EDDnp <sup>24-26</sup>	20	30	320	420

\* pro-MMP1 was activated by incubation for 2 h at 37 °C in the presence of 1 mM final 4-aminophenylmercuric acetate (AMPA, 100 mM stock in DMSO).

### Supplementary Table 6.

Specificity profiling performed by EuroFins (Panlabs) for substrate-selective IDE inhibitor **63** (1 and 10  $\mu$ M final concentration) using the approximately equipotent zinc-chelating IDE inhibitor **li1** (**2**) (1  $\mu$ M) for comparison<sup>18,27</sup>.

<b>Eurofins Assay #</b>	<b>Enzyme assay (relative signal to DMSO control)*</b>	<b>li1 (1 <math>\mu</math>M)*</b>	<b>43 (1 <math>\mu</math>M)</b>	<b>43 (10 <math>\mu</math>M)</b>
112250	Cathepsin B Human Papain Cysteine Peptidase	4%	1%	3%
112350	Cathepsin D Human Pepsin Aspartic Peptidase	$\leq 0\%$	$\leq 0\%$	0%
199007	DPP4 Dipeptidyl Peptidase 4 Human Prolyl Oligopeptidase	$\leq 0\%$	$\leq 0\%$	$\leq 0\%$
163950	ECE1 Human Neprilysin Metallo Peptidase	$\leq 0\%$	2%	5%
114110	MMP1 Human Matrix Metallopeptidase	0%	$\leq 0\%$	1%
114210	MMP2 Human Matrix Metallopeptidase	22%	1%	5%
114310	MMP3 Human Matrix Metallopeptidase	6%	1%	1%
114710	MMP7 Human Matrix Metallopeptidase	8%	$\leq 0\%$	1%
114800	MMP8 Human Matrix Metallopeptidase	22%	$\leq 0\%$	$\leq 0\%$
114910	MMP9 Human Matrix Metallopeptidase	3%	$\leq 0\%$	$\leq 0\%$
114950	MMP10 Human Matrix Metallopeptidase	10%	0%	5%
115200	MMP12 Human Matrix Metallopeptidase	98%	6%	6%
115300	MMP13 Human Matrix Metallopeptidase	14%	3%	6%
115400	MMP14 Human Matrix Metallopeptidase	16%	1%	2%
115450	MMP15 Human Matrix Metallopeptidase	9%	$\leq 0\%$	$\leq 0\%$
115490	MMP17 Human Matrix Metallopeptidase	1%	$\leq 0\%$	0%
115510	MMP19 Human Matrix Metallopeptidase	2%	$\leq 0\%$	4%
115520	MMP20 Human Matrix Metallopeptidase	2%	$\leq 0\%$	3%
115560	MMP24 Human Matrix Metallopeptidase	46%	1%	30%
164010	Neutral Endopeptidase Human Neprilysin Metallo Peptidase	$\leq 0\%$	$\leq 0\%$	$\leq 0\%$
166500	TACE Human Astacin/Adamalysin Metallo Peptidase	34%	1%	8%

\* For additional comparisons with the specificity profile in Fig. 2I, see also reference 18 that includes specificity data for **li1** inhibition of neurolysin (NLN), thimet oligopeptidase (THOP), neprilysin (NEP), matrix metalloprotease-1 (MMP1), and angiotensin-converting enzyme (ACE) under similar conditions.

**Supplementary Table 7.**

Data collected was obtained from one crystal. Statistics for the highest resolution shell are shown in parentheses. Coordinates for the IDE-•37, IDE•63, and IDE•63•glucagon co-crystal structures are deposited in the Protein Data Bank under the accession codes 6BYZ, 6EDS, and 6MQ3, respectively.

<b>Data collection</b>	<b>IDE•37 (PDB ID 6BYZ)*</b>	<b>IDE•63•glucagon (PDB ID 6EDS)*</b>	<b>IDE•63 (PDB ID 6MQ3)*</b>
Space group	P6 <sub>5</sub>	P6 <sub>5</sub>	P6 <sub>5</sub>
Cell dimensions			
<i>a, b, c</i> (Å)	264.49, 264.49, 91.09	263.12, 263.12, 90.32	263.25, 263.25, 91.23
$\alpha, \beta, \gamma$ (°)	90, 90, 120	90, 90, 120	90, 90, 120
Resolution range (Å)	48.48 - 2.956 (3.062 – 2.956)	131.56 - 3.18 (3.24 – 3.18)	63.23 - 3.57 (3.70 – 3.57)
R <sub>merge</sub>	0.1894 (1.318)	0.369 (1.897)	0.108 (0.352)
<i>I</i> / $\sigma$ <i>I</i>	16.34 (1.91)	10.8 (2.1)	6.85 (2.41)
Completeness (%)	99.84 (98.88)	100.0 (100.0)	99.9 (100.0)
Redundancy	12.4 (10.9)	20.9 (21.1)	4.7 (4.6)
<b>Refinement</b>			
Resolution (Å)	2.96	3.18	3.57
No. reflections	76278	60302	43243
R <sub>work</sub> / R <sub>free</sub>	0.161/0.203	0.177/0.222	0.162/0.211
No. of atoms			
protein	15653	15800	15596
ligand/ion	108	126	100
solvent	389	-	-
B-factors			
protein	60.57	51.12	70.91
ligand/ion	73.84	71.63	88.29
water	58.75	-	-
R.M.S. deviations (bonds)	0.006	0.004	0.002
R.M.S. deviations (angles)	0.84	0.64	0.48

\* Data collected was obtained from one crystal. Statistics for the highest resolution shell are shown in parentheses.

**Supplementary Table 8.**

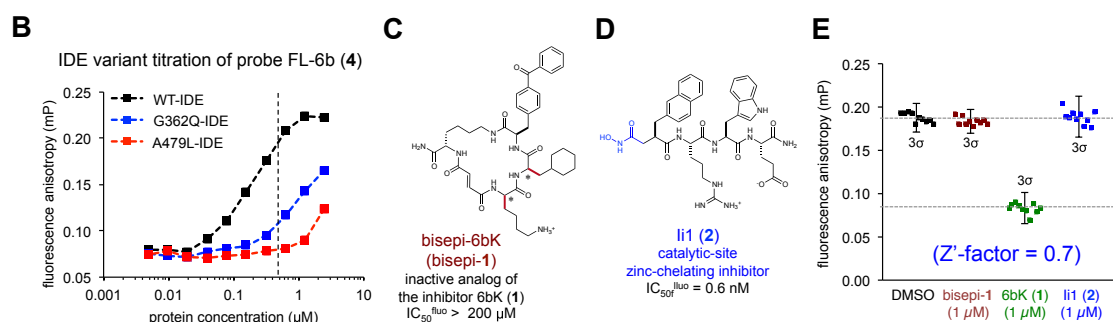
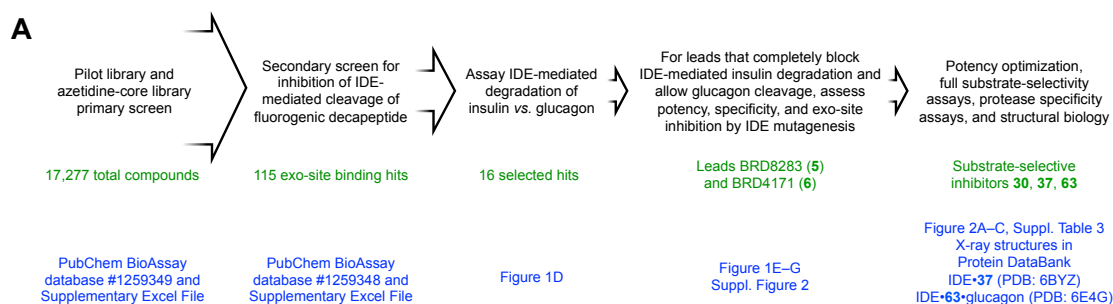
Site-directed mutagenesis primers.

<b>Mutation</b>	<b>Primers (forward, reverse)</b>
A198T	AGACTCTTTCAATTGGAAAAAGC-dU-ACAGGG AGCTTTTTCCAATTGAAAGAGTC-dU-CCAGGTATCATTCATCACATTCTTCTCATGTTC
W199F	AGACTCTTTCAATTGGAAAAAGC-dU-ACAGGG AGCTTTTTCCAATTGAAAGAGTC-dU-GAAGGCATCATTCATCACATTCTTCTC
F202R	AGACTCTTTCAATTGGAAAAAGC-dU-ACAGGG ATGAATGATGCCTGGAGAC-dU-CCGTCAATTGGAAAAAGCTACAGGG
Y314F	ACCCATTAAGATATTAGGAATCTC-dU-TCGTGACATTTCCCATACCTGACCTTC AGAGATTCCTAATATCTTTAATGGG-dU-ACTATTTTG
V360Q	AAAGGGCTGGGTAAATACTCT-dU-CAGGGTGGGCAG AAGAGTATTAACCCAGCCCTT-dU-GACTTAAG
G362Q	AAAGGGCTGGGTAAATACTCT-dU-GTTGGTCAGCAGAAGGAAGGAGCCCGAG AAGAGTATTAACCCAGCCCTT-dU-GACTTAAG
I374Q	ATGTTTTTTCAGATTAATGTGGACT-dU-GACCGAGGAAGG AAGTCCACATTAATCTGAAAAACA-dU-AAAACCTCGGGCTCCTTC
A479L	ATGTCCGGGTCTGATAGTTTCTAAA-dU-CTTTTGAAGGAAAAACTG ATTTAGAACTATCAGAACCCGGACA-dU-TTCTGGTCTGAG

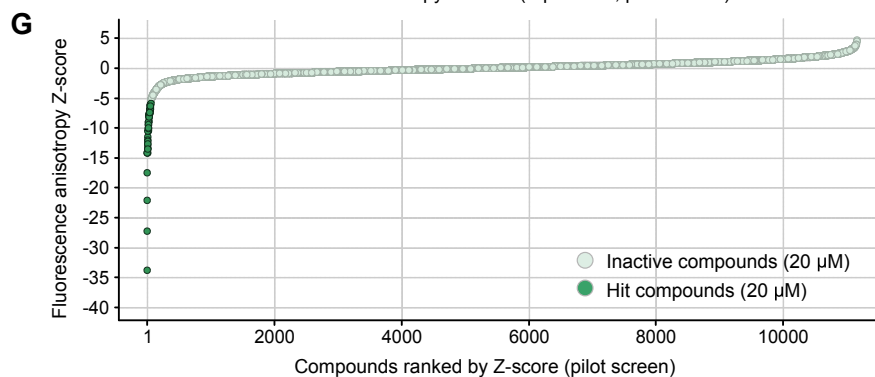
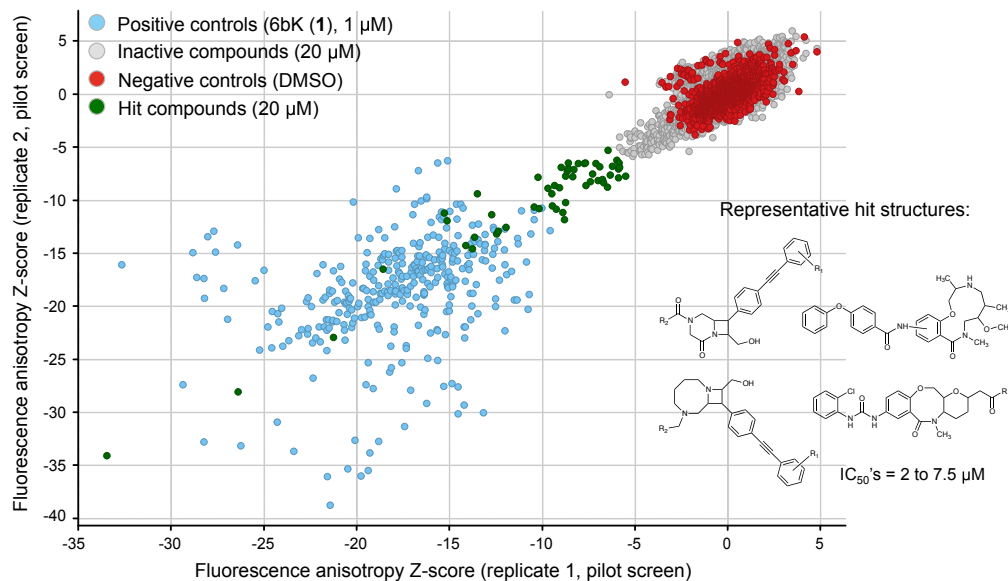
**Supplementary Table 9.**Data collected was obtained from one crystal of synthetic intermediate **66**.

Data collection	Intermediate 66 ( <i>JP-175</i> )
<b>Crystal data</b>	
Chemical formula	C <sub>40</sub> H <sub>36</sub> BrF <sub>3</sub> N <sub>2</sub> O <sub>3</sub> S
<i>M<sub>r</sub></i>	761.68
Crystal system, space group	Triclinic, <i>P</i> 1
Temperature (K)	100
<i>a</i> , <i>b</i> , <i>c</i> (Å)	8.9875 (5), 9.3004 (6), 11.7462 (7)
$\alpha$ , $\beta$ , $\gamma$ (°)	98.6654 (10), 111.3696 (9), 91.0394 (10)
<i>V</i> (Å <sup>3</sup> )	901.04 (9)
<i>Z</i>	1
Radiation type	Mo K $\alpha$
$\mu$ (mm <sup>-1</sup> )	1.25
Crystal size (mm)	0.18 × 0.14 × 0.12
<b>Data collection</b>	
Diffractometer	Bruker D8 goniometer with CCD area detector diffractometer
Absorption correction	Multi-scan <i>SADABS</i>
<i>T<sub>min</sub></i> , <i>T<sub>max</sub></i>	0.834, 0.862
No. of measured, independent and observed [ <i>I</i> > 2 $\sigma$ ( <i>I</i> )] reflections	12958, 7482, 7200
<i>R<sub>int</sub></i>	0.016
( <i>sin</i> $\theta$ / $\lambda$ ) <sub>max</sub> (Å <sup>-1</sup> )	0.641
<b>Refinement</b>	
<i>R</i> [ <i>F</i> <sup>2</sup> > 2 $\sigma$ ( <i>F</i> <sup>2</sup> )], <i>wR</i> ( <i>F</i> <sup>2</sup> ), <i>S</i>	0.027, 0.057, 1.04
No. of reflections	7482
No. of parameters	455
No. of restraints	3
H-atom treatment	H atoms treated by a mixture of independent and constrained refinement
$\Delta\rho_{\max}$ , $\Delta\rho_{\min}$ (e Å <sup>-3</sup> )	0.45, -0.22
Absolute structure	Flack <i>x</i> determined using 3211 quotients [( <i>I</i> <sup>+)-(<i>I</i><sup>-</sup>)]/[(<i>I</i><sup>+</sup>)+(<i>I</i><sup>-</sup>)] (Parsons, Flack and Wagner, <i>Acta Cryst.</i> B69 (2013) 249-259).</sup>
Absolute structure parameter	-0.008 (3)

Computer programs: *APEX2* v2014.3.0<sup>28</sup>, *SAINT* 8.34C<sup>28</sup>, *SHELXT*-2014<sup>29</sup>, *SHELXL2014*<sup>30</sup>, Bruker *SHELXTL*<sup>30</sup>.

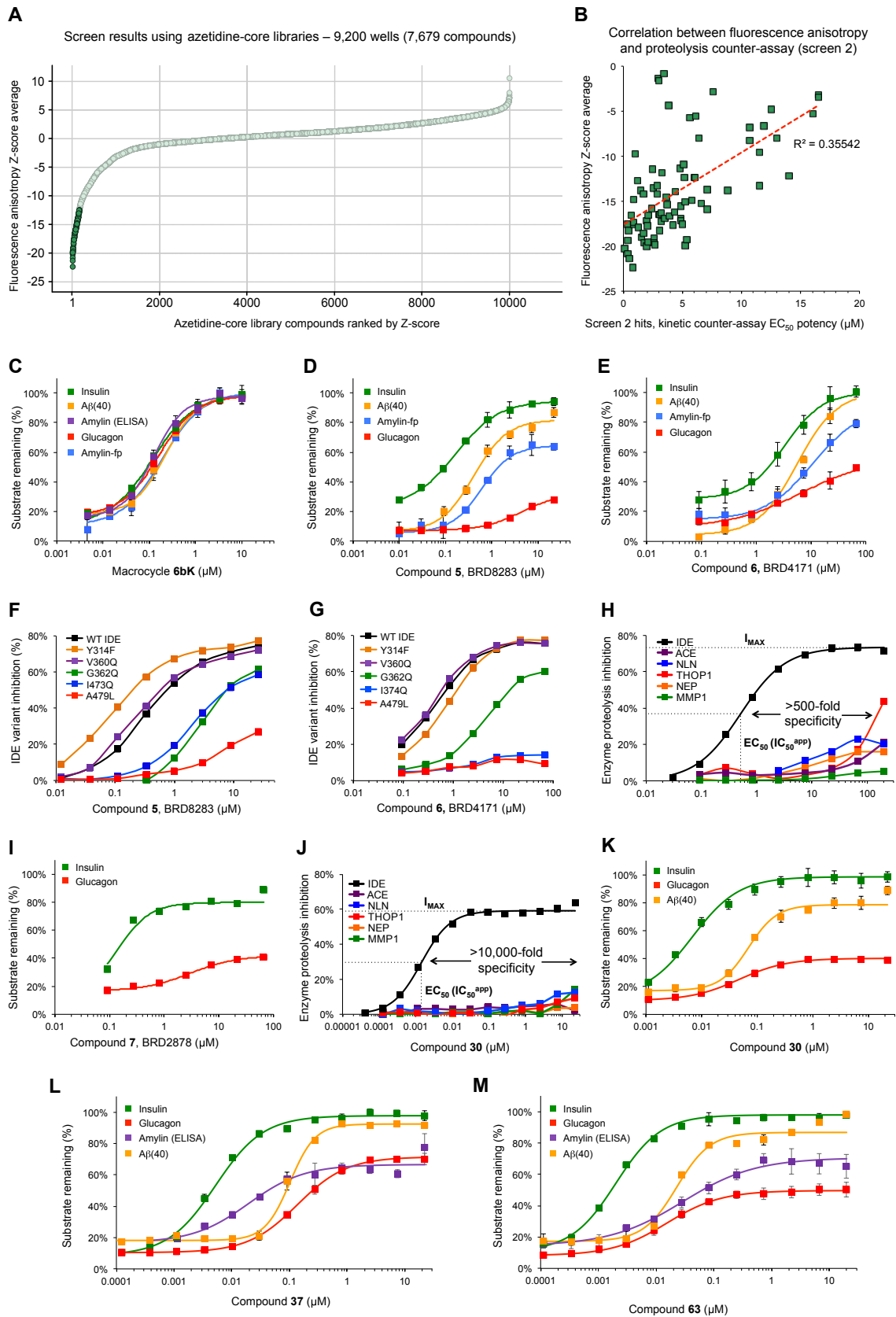


**F** Pilot screen using the Broad Institute “DOS Informer Set” – 11,520 wells (9,598 compounds)



**Supplementary Fig. 1** | (A) Flow chart of high-throughput screen and secondary assays used in this study<sup>18</sup>. (B) Complementary assay supporting the specificity of FL-6b (4) for the exo site of IDE was performed by

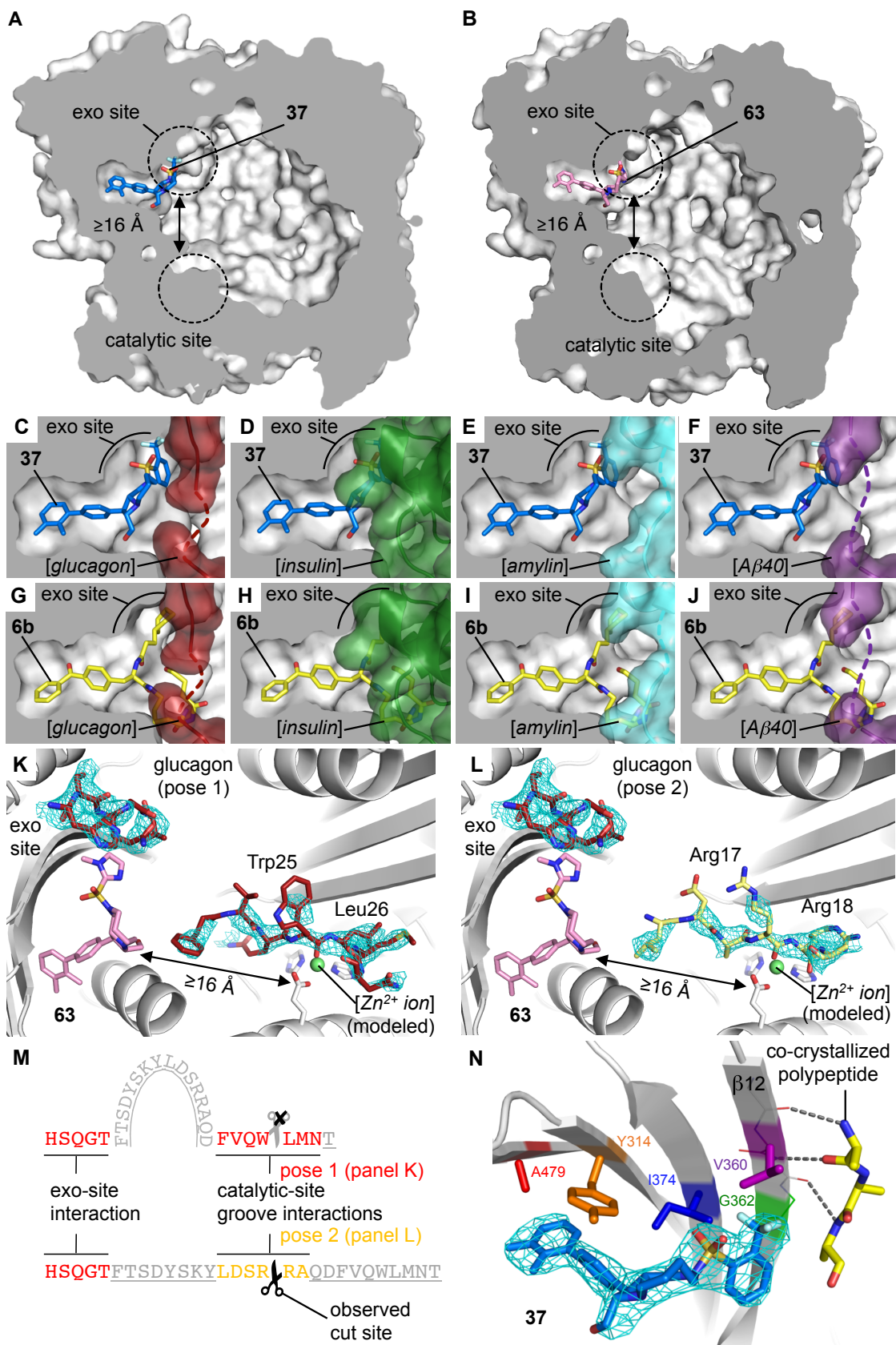
titrating the FL-6b (**4**) fluorescence anisotropy signal with increasing concentrations of wild-type N-His<sub>6</sub>-IDE<sub>42-1019</sub> (■) or the mutant IDE variants Ala479→Leu (■) and Gly362→Gln (■), which occlude the exo site<sup>18</sup>. The points represent averages of three technical replicates, and the dashed line indicates 0.5 μM protein, which was the concentration selected for the high-throughput screen. (C–D) Structures of the inactive bisepimer of 6bK used as a negative control (**bisepi-1**, IC<sub>50</sub> > 200 μM)<sup>18</sup> and the zinc-chelating tetrapeptide Ii1 (**2**) with the hydroxamic acid group that binds the catalytic zinc of IDE shown in red<sup>27</sup>. (E) Z'-score calculated for 16 technical replicates per condition, with error bars set to 3xSD to convey the signal-to-noise ratio. The anisotropy measurement for IDE-bound FL-6b (**4**) (high anisotropy indicated with the upper dashed line) is observed to diminish in the presence of the exo-site inhibitor 6bK (**1**) (1 μM, low anisotropy indicated with the lower dashed line), but not by addition of the low affinity/inactive bisepi-6bK (**bisepi-1**, 1 μM)<sup>18</sup>. The potent IDE inhibitor Ii1 (**2**) (1 μM), which binds the catalytic site by chelating zinc, does not displace FL-6b (**4**) and does not cause an decrease in fluorescence anisotropy (Z'-factor = 0.7). Additionally, the Z'-factor = 0.7 was confirmed using the mean and standard deviations of the DMSO controls and 6bK (**1**) positive controls in a full 384-well plate (n = 192 each)<sup>31</sup>. (F) Pilot high-throughput screen using the “DOS Informer Set”, a collection of 25 selected 384-well plates representative of small-molecule libraries at the Broad Institute (PubMed BioAssay AID: 1259349). The pilot screen used 11,520 wells carrying N-His<sub>6</sub>-IDE<sub>42-1019</sub> (0.5 μM) and fluorescent probe FL-6b (**4**) (30 nM), followed by pinning compound plates and 6bK (**1**) positive control plates (● “DOS Informer Set” compounds, ● 1,561 DMSO negative controls, and ● 360 6bK (**1**) positive control wells). The screen was performed in duplicate (X/Y values), and the anisotropy signal was used to calculate normalized Z-scores based on the negative controls of each plate. The top 20 compounds highlighted (●) displayed low anisotropy signal for FL-6b (**4**) (Z-score < -12 in replicate plates) compared to negative controls and inactive compounds (●). The structures and counter-screen EC<sub>50</sub> values for the cherry-picked compounds are deposited in PubChem BioAssay database #1259348. (G) Rank-ordered plot of Z-score values (averages of the two technical replicates) for the pilot screen, highlighting in dark green the same compounds as in panel F (negative and positive controls are not included in this plot).



**Supplementary Fig. 2 | (A)** Rank-ordered plot of Z-score values (averages of the two technical replicates) for the focused screen of azetidine-core library members, highlighting in dark green the same compounds as in

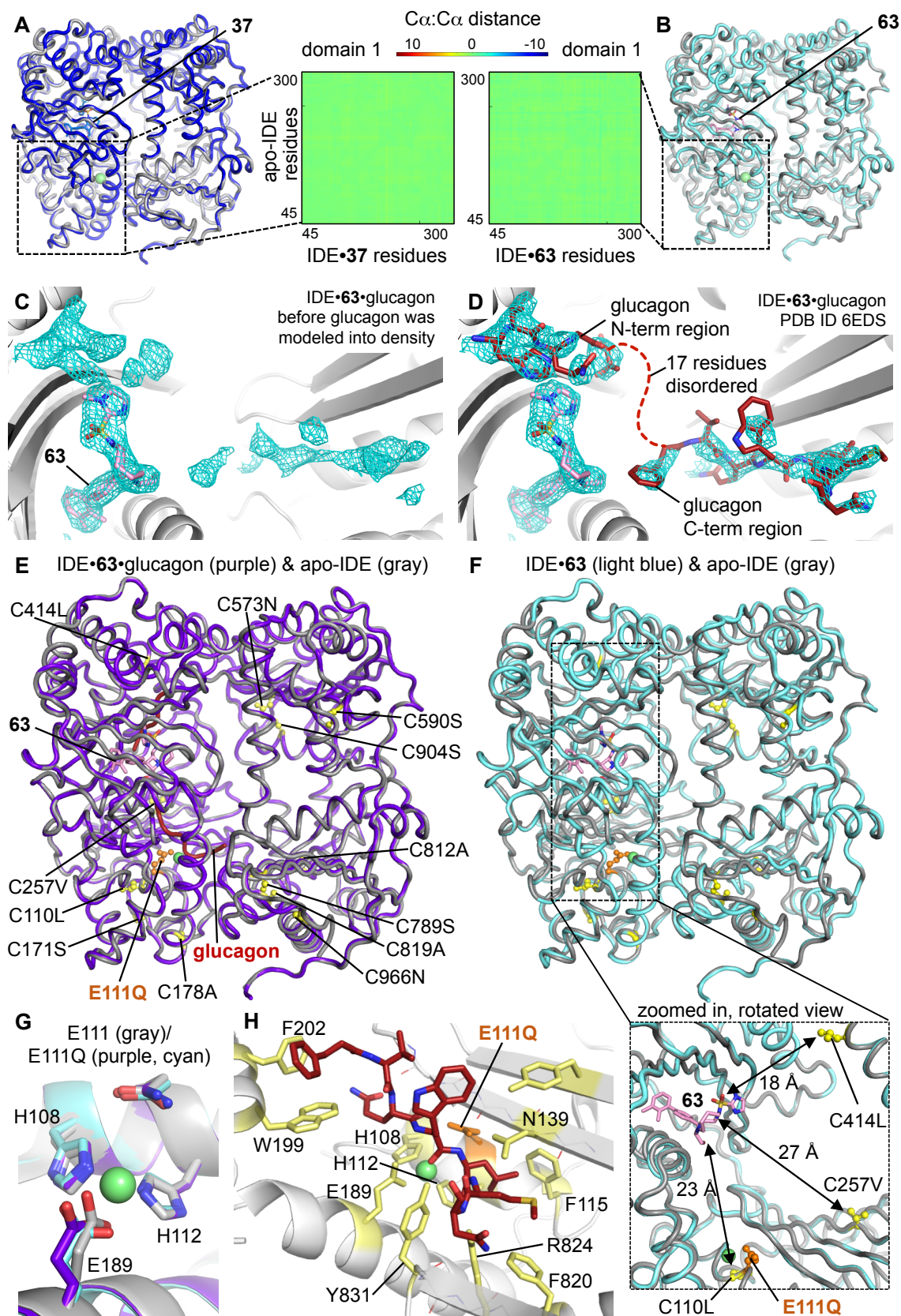


Fig. 1C (negative and positive controls are not included in this plot). **(B)** Correlation between fluorescence anisotropy of FL-6b (**4**) displacement Z-scores and EC<sub>50</sub> values (capped at 20 μM) for all library compounds tested in this study (n = 81). The points represent averages of two technical replicates, and the trend-line reflects the linear regression fit (R<sup>2</sup> = 0.355). **(C–E)** We selected the most promising substrate-selective hits to determine the IDE-mediated degradation assays with other IDE substrates in the presence of 6bK (**1**), BRD8283 (**5**), and BRD4171 (**6**), respectively. Aβ40 (**■**) was assayed using the same HTRF system used for insulin and glucagon. Since paired antibody assays were not available for amylin, we used a surrogate fluorogenic peptide “Amylin-fp” (**■**) (KCNTATCATXRLANFLVHSSNNZGAILSSTNVGSNTY-NH<sub>2</sub>, in which X = Lys-γN-anthranilamide and Z = *m*-nitrotyrosine) based on the human amylin sequence (KCNTATCATQRLANFLVHSSNNFGAILSSTNVG SNTY-NH<sub>2</sub>) and at a later stage of the study we optimized an ELISA-based assay for IDE-mediated degradation of amylin (**■**, unmodified, full length). The amylin substrate assays produce similar EC<sub>50</sub> results with 6bK (**C**). **(F–G)** Confirmation of the distal binding site for the substrate-selective hits BRD8283 (**5**) and BRD4171 (**6**, BRD-K20484171-001-01-8) by comparing inhibition potencies against wild-type IDE (**●**) and mutant His<sub>6</sub>-IDE variants expressed in *E. coli*, previously shown to affect 6bK (**1**)<sup>18</sup>: A479L (**■**), I374Q (**■**), G362Q (**■**), V360Q (**■**) and Y314F (**■**). See Figure 5E for residue positions. Points represent averages of two technical replicates. **(H)** Metalloprotease specificity profile for the substrate-selective hit BRD4171 (**6**, BRD-K20484171-001-01-8) using thimet oligopeptidase (**■**, THOP), neurolysin (**■**, NLN), neprilysin (**■**, NEP), matrix metalloprotease 1 (**■**, MMP1), and angiotensin converting-enzyme (**■**, ACE). **(I)** IDE mediated-degradation of insulin and glucagon in the presence of hit BRD2878 (**7**). **(J)** The same metalloprotease specificity panel as above for the *ortho*-methyl locked-biaryl analog of BRD8283, compound **30** (Supplementary Figure 2A,D). The dotted lines in panels H and J show the percentage inhibition maximum (I<sub>MAX</sub>) and the relative EC<sub>50</sub> (or apparent IC<sub>50</sub><sup>app</sup>) determined from the kinetic mode proteolysis assay using the fluorogenic decapeptide substrate Mca-RPPGFSAFK(Dnp)-OH. **(K–M)** We assayed IDE-mediated degradation of amylin (**■**) and Aβ40 (**■**) for compounds **37** (**L**) and **63** (**M**), shown overlaid with the respective insulin (**■**) and glucagon (**■**) profiles as in Fig. 3B–C, and for compound **30** (**K**) shown overlaid with Aβ40 (**■**). Values and error bars reflect mean ± SEM of three technical replicates (**C–E**, **K–M**) or two technical replicates in the assays using IDE variants and the additional metalloprotease proteins (**F–J**).



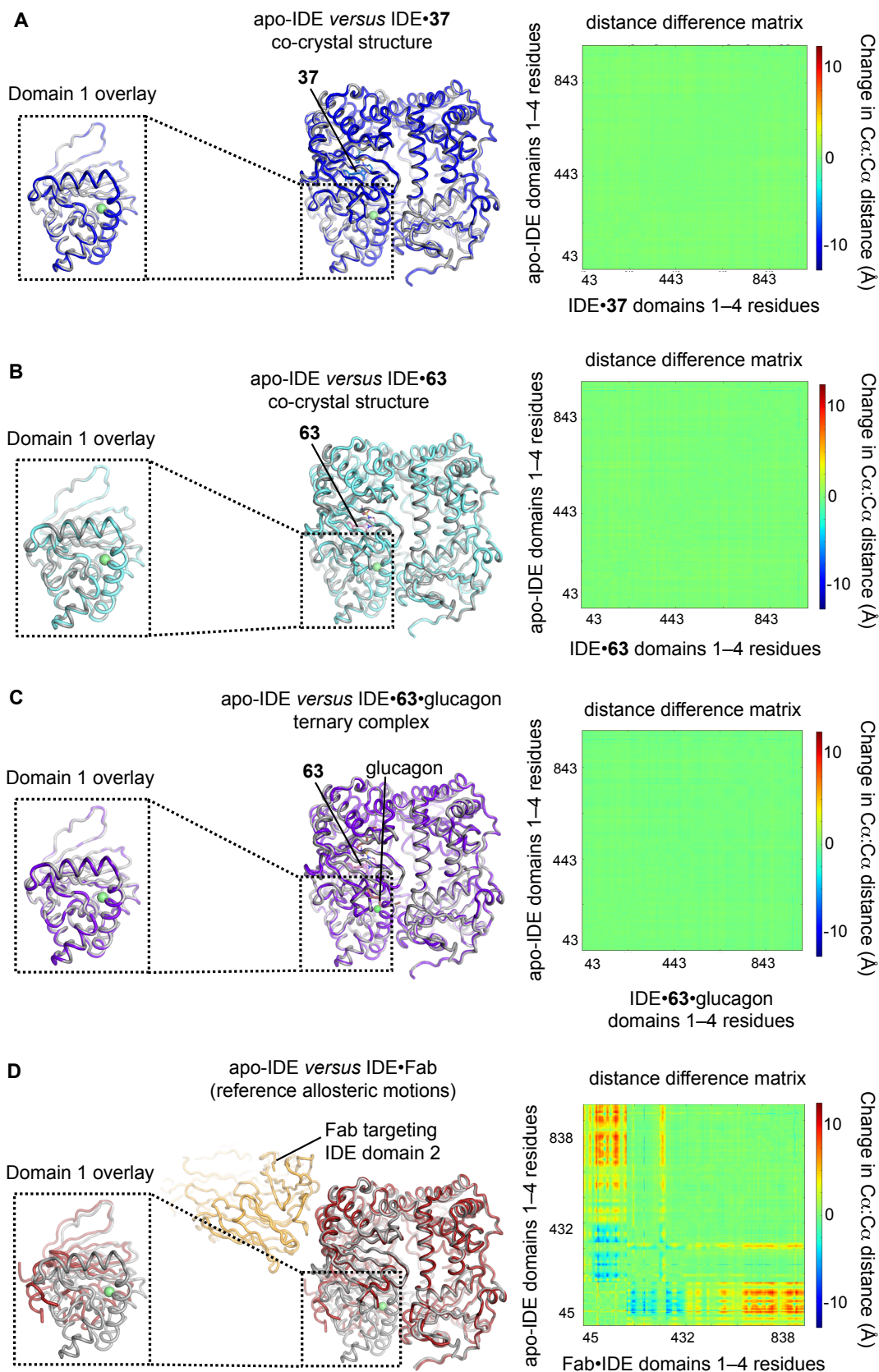
**Supplementary Fig. 3** | Structural basis for substrate selective small molecule inhibition of IDE by compounds 37 and 63. (A–B) X-ray co-crystal structure of 37 and 63 bound to IDE (PDB ID 6BYZ, 2.96 Å

resolution, and PDB ID 6MQ3, 3.57 Å resolution, respectively, see Supplementary Table 7). (C–J) Exo-site view of IDE•**37** (left panels, C–F) and IDE•**6b (3)** (right panels, G–J) overlaid with known substrate•IDE co-crystal structures, top to bottom: glucagon (red surface; from the IDE•**63**•glucagon structure PDB ID 6EDS), insulin (green surface; PDB ID 2WBY), amylin (PDB ID 2G48; cyan surface), and amyloid-β(1–40) (PDB ID 2G47; purple surface)<sup>32</sup>. Dashed lines represent unresolved residues for each peptide substrate, and all the superimposed models are labeled in square brackets. These structural models are consistent with the observed non-substrate-selective competitive inhibition for all IDE substrates by the macrocyclic IDE inhibitors **6b (3)** and the analog **6bK (1)** (Figure 1E). (K–L) The electron density map for the C-terminal residues of glucagon (mesh contoured at 1σ) permit the modeling of two alternative poses for the catalytic groove interactions of the IDE•**63**•glucagon ternary complex, which are consistent with the prior IDE•glucagon structure (PDB ID 2G49, binding pose 1) or the primary cleavage site observations (Supplementary Figure 6, cleavage-competent pose 2), respectively. (K) This glucagon binding pose is obtained using the reported IDE•glucagon structure as a guide (PDB ID 2G49), in which glucagon residues 22–27 were modeled in the catalytic site (FVQWLM). (L) The cleavage-competent pose is obtained by modeling glucagon residues 14–19 (LDSRRA) into the catalytic site, which places Arg17 and Arg18 positioned next to the zinc atom (modeled based on PDB structure 4LTE). (M) Linear representation of the glucagon binding pose 1 and cleavage-competent pose 2, where the grey underlined text corresponds to unresolved residues that were not modeled into the electron density map, and the red/yellow color corresponds to the glucagon residues modeled in panels K and L, respectively. (N) Co-crystallized polypeptide, modeled as (Ala)<sub>3</sub> within the cavity of the IDE•**37** structure interacting with beta-sheet β12 of IDE's exo site. The mesh represents the composite omit electron density map of ligand **37** contoured at 1σ. The exo-site residues are highlighted with colors that match Fig. 1I. The co-crystals Glu111Gln-IDE•**63**•glucagon and Glu111Gln-IDE•**37** were zinc-free, as observed in previous IDE co-crystal structures PDB IDs 2G47, 2G48, 2G49 and 2G56; therefore, we used our previously solved IDE•**6b (3)** structure (PDB ID 4LTE) to model the zinc ion (green sphere) in the catalytic site as shown in the panels above. The catalytic site residues His108, His112, and Glu189 were found in the expected poses for coordinating a zinc ion in the IDE•**63**•glucagon and IDE•**37** structures. The double-arrow in panels M and N indicates that the nearest atom of ligands **63** and **37** is located ≥16.2 Å from the nearest catalytic residue and ≈17.8 Å from the modeled zinc ion.



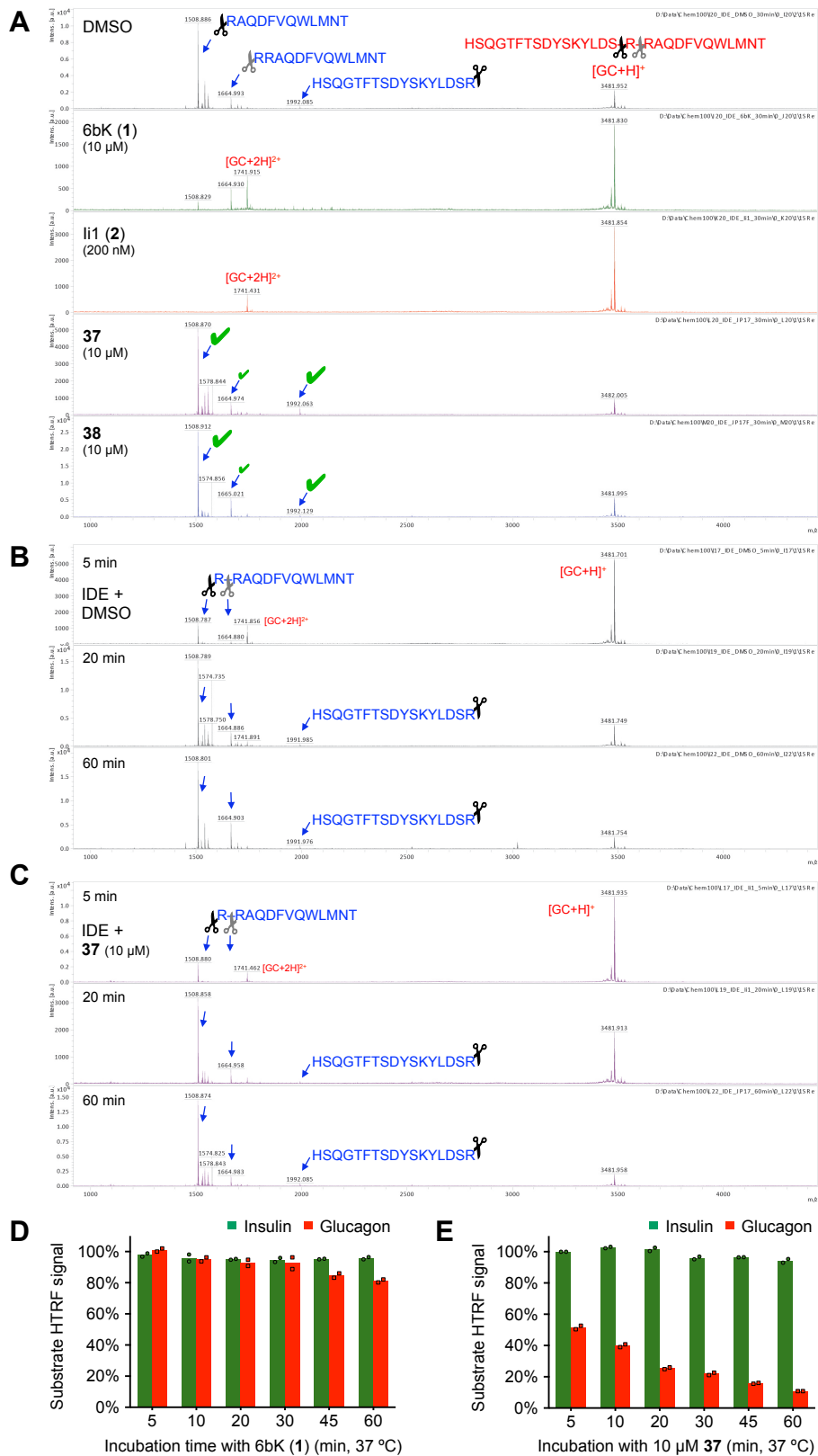
**Supplementary Fig. 4** | Substrate selective inhibition of IDE by compounds **37** and **63** does not induce significant conformational changes or allosteric effects on the catalytic site. (**A–B**) Distance difference

matrix showing changes in domain 1 C $\alpha$ :C $\alpha$  distances between apo-IDE (PDB ID 2JG4, gray) and IDE•**37** residues (**A**, blue) and IDE•**63** residues (**B**, cyan). (**C**) The 2FoFc map (contoured at 1 $\sigma$ ) from an early IDE•**63**•glucagon structure refinement before glucagon was modeled into IDE revealed prominent electron density in the IDE cavity that we predicted corresponded to glucagon. (**D**) The final model of glucagon in our refined structure (PDB ID 6EDS, see also Supplementary Fig. 3K). A previously solved co-crystal structure of IDE•glucagon (PDB ID 2G49) was used to guide building this structural model (Supplementary Fig. 3L shows a view of a cleavage-competent pose of the C-terminal region of glucagon that can also be feasibly modeled into the electron density within IDE). (**E–G**) All the IDE co-crystal structures containing inhibitors **37** and **63** were generated using a catalytically inactive Glu111Gln cysteine-free IDE mutant (CF-IDE-E111Q), which is a well-established IDE form for structural studies with IDE substrates. (**E–F**) Overlay of catalytically active apo-IDE Y831F with all cysteines intact (gray, PDB ID 2JG4) and either IDE•**63**•glucagon (**E**, purple ribbon, PDB ID 6EDS, RMSD = 0.273 Å) or IDE•**63** (**F**, cyan ribbon, PDB ID 6MQ3, RMSD = 0.319 Å) reveals that both CF-IDE-E111Q co-crystal structures possess an identical closed conformation to apo-IDE. Mutated cysteine residues are labeled and highlighted as yellow spheres, as resolved in the CF-IDE-E111Q co-crystal structures. Zoomed-in view of panel D shows that the cysteine mutations C257V, C414L, and C110L, which are closest in proximity to **63**, stand at considerable distances ranging from  $\geq 18$  to 27 Å, and are not predicted to impact **63** binding at the exo site. (**G**) Overlay of catalytic sites between active apo-IDE containing wildtype Glu111 (gray; PDB ID 2JG4), and catalytically inactive IDE•**63** (cyan, PDB ID 6MQ3) and IDE•**63**•glucagon (purple, PDB ID 6EDS) reveal that, as expected, the catalytic residues across all three co-crystal structures bear similar orientation. (**H**) Interactions between CF-E111Q-IDE and the C-terminal residues of glucagon (PDB ID 6EDS), show that the E111Q mutation does not directly contact the glucagon substrate. CF-IDE residues that make electrostatic contacts with glucagon (red sticks) are highlighted as yellow sticks, and protein backbone interacting atoms are illustrated in thin lines.



**Supplementary Fig. 5** | Analysis of IDE X-ray co-crystal protein conformations and residue motions compared to apo-IDE. (A–D) Left: zoom on domain 1 overlays for the distance difference matrix (DDM) plots shown in Fig. 5A–B and Supplementary Fig. 4. Middle: paired overlays of the complete IDE protein

chains. Right: DDM plots summarizing the relative difference in  $C\alpha$ - $C\alpha$  distances between the superimpositions of all resolved residues (43/45–1011) of domains 1–4 of IDE using apo-IDE as the reference (PDB ID 2JG4, gray ribbons). For comparison, the calculations shown in Fig. 5A–B are specific for intra-domain 1 motions among residues 45–300, and do not reflect relative domain–domain motions, as reflected in this figure. **(A–B)** Structural comparison of the full-length of IDE alone *versus* IDE bound by ligand **37** (gray *versus* blue ribbon, **A**) or IDE bound by ligand **63** (gray *versus* cyan ribbon, **B**) both suggest the exo-site inhibitor causes negligible allosteric adjustments on the neighboring domain 1, an observation further supported by a DDM plot featuring minimal differences in  $C\alpha$ - $C\alpha$  distances between the two structures. **(C)** Structural comparison of IDE alone *versus* IDE•**63**•glucagon (gray *versus* purple ribbon), together with a virtually featureless DDM plot, suggest that the ternary complex possesses negligible allosteric adjustments on IDE's domain 1 and highlights the complex's conformational similarity to cleavage-competent apo-IDE. **(D)** Reference inhibitory allosteric motions of domain 1 produced by conformational allostery from an antibody fragment (Fab, yellow ribbon) bound on the outer surface of IDE's domain 2 (PDB ID 4IOF, red ribbon, compared to IDE alone in grey ribbon)<sup>33</sup>. The reference DDM plot shows residue motions concentrated in the catalytic groove and floor subdomain<sup>33</sup>. The overall analysis suggests that substrate-selective exo-site ligands do not induce obvious changes in IDE protein conformation or allosteric motions in IDE domain 1 residues 45–285 (floor subdomain, or catalytic site). These calculations support the notion that exo-site binding inhibitors do not interact with cation-binding residues of IDE by direct or allosteric mechanisms.



**Supplementary Fig. 6 | (A)** Substrate-selective IDE inhibitors do not alter the sites of glucagon cleavage. IDE reactions were prepared with human glucagon (Eli Lilly) in the presence of macrocyclic inhibitor 6bK (1) (10  $\mu$ M), zinc chelator Ii1 (2) (200 nM) or substrate-selective inhibitors **37** and **38** (both 10  $\mu$ M, 10,000x



and 400x the respective EC<sub>50</sub> concentrations), followed by quenching with 0.5% TFA. The MALDI-TOF instrument was calibrated using five peptide standards: bradykinin<sub>(1-7)</sub>, angiotensin-II, P<sub>14</sub>R, ACTH<sub>(18-39)</sub> and bovine insulin oxidized B-chain. We observed glucagon starting material as singly- and doubly-charged ions (red labels). The pattern of glucagon cleavage products was unchanged in the presence of saturating concentration of ligand **37** (10 μM) or ligand **38** (10 μM) compared to IDE in the absence of any inhibitor. The following ions were assigned to the major and minor IDE cleavage products of glucagon (blue labels), which were consistent with the cleavage products previously observed<sup>32,34</sup>: \*RAQDFVQWLMNT calculated [M+H]<sup>+</sup> = 1508.7315, observed = 1508.85 (average), Δ = -78.5 ppm; \*RRAQDFVQWLMNT calculated [M+H]<sup>+</sup> = 1664.8326, observed = 1664.95 (average), Δ = -70.5 ppm; and HSQGTFTSDYSKYLDSR\* calculated [M+H]<sup>+</sup> = 1991.9094, observed 1992.05 (average), Δ = -70.6 ppm. Starting material ions for glucagon: HSQGTFTSDYSKYLDSRRAQDFVQWLMNT calculated [M+H]<sup>+</sup> = 3481.6230 and [M+2H]<sup>2+</sup> = 1741.3151, found 3481.88 and 1741.66 (averages), Δ = -73.8 and -198 ppm, respectively. (B, C) Qualitative MALDI-TOF time course of glucagon cleavage reactions in the presence of **37** (10 μM, 10,000x EC<sub>50</sub>) or IDE in the absence of inhibitor (DMSO control) based on the relative ion intensities. The MALDI-TOF spectra are representative results from two similar trials. (D–E) Extending the incubation period for up to one hour does not lead to insulin degradation (■, 1.7 nM) using human IDE at 37 °C in the presence of 6bK (**1**) (5 μM) or the substrate-selective inhibitor **37** (10 μM), whereas only the latter treatment leads to glucagon depletion (■, 1.2 nM). Aliquots of each reaction were quenched at the specified times using Ii1 (**1**) (200 nM) followed by HTRF dual-antibody assays for each substrate hormone. For comparison, the optimized glucagon degradation assays in Fig. 2B–C used 10-min incubations at room temperature, and insulin incubation were 15 min at 30 °C, as described in the Online Methods section. Values represent two technical replicates.

#### **Supplementary Data Set 1. (separate file)**

Supplementary data deposited in PubMed BioAssay “Supplementary Data Set 1 (PubChem BioAssay data, Maianti et al).xlsx”. This Microsoft Excel file has 3 spreadsheets under the following tabs: “IDE pilot screen 1”, “IDE azetidine library screen 2”, and “IDE proteolysis counter-screen results”. All entries have a unique Broad ID, PubChem SID and CID identifiers for each compound, and the SMILES code for the chemical structure. The high-throughput anisotropy screen data has been deposited in PubMed BioAssay AID: 1259349 (n = 17,277 compounds) and the counter-screen IDE inhibition data in PubMed BioAssay AID: 1259348 (n = 115 compounds).

#### **Supplementary Data Set 2. (separate file)**

Supplementary reports and data provided by EuroFins (Belgium) that is summarized in Supplementary Table 6 “Supplementary Data Set 2 (Protease Specificity Panel Reports from EuroFins, Maianti et al).pdf”.

#### **Supplementary Data Set 3. (separate file)**

Nuclear Magnetic Resonance spectra (<sup>1</sup>H-, <sup>13</sup>C-, and <sup>19</sup>F-NMR) “Supplementary Data Set 3 (NMR spectra, Maianti et al).pdf”.

#### **Supplementary Video. (separate file)**

Supplementary animation generated using PyMol (1,000 frames) “Supplementary Video (IDE-63-glucagon ternary complex X-ray structure 6EDS, Maianti et al).mov”.

#### **Supplementary Note. (separate file)**

Synthetic procedures and Nuclear Magnetic Resonance spectra descriptions “Supplementary Note (Maianti Liu et al).docx”. See Supplementary Data Set 3 for NMR spectra.

## Supplementary References

- 1 Busschots, K. *et al.* Substrate-selective inhibition of protein kinase PDK1 by small compounds that bind to the PIF-pocket allosteric docking site. *Chem Biol* **19**, 1152-1163, (2012).
- 2 Knight, Z. A. For a PDK1 inhibitor, the substrate matters. *Biochem J* **433**, e1-2, (2011).
- 3 Rettenmaier, T. J. *et al.* A small-molecule mimic of a peptide docking motif inhibits the protein kinase PDK1. *Proc Natl Acad Sci U S A* **111**, 18590-18595, (2014).
- 4 Knapinska, A. M. *et al.* SAR Studies of Exosite-Binding Substrate-Selective Inhibitors of A Disintegrin And Metalloprotease 17 (ADAM17) and Application as Selective in Vitro Probes. *J Med Chem* **58**, 5808-5824, (2015).
- 5 Madoux, F. *et al.* Discovery of an enzyme and substrate selective inhibitor of ADAM10 using an exosite-binding glycosylated substrate. *Scientific reports* **6**, 11, (2016).
- 6 Berg, D. T., Wiley, M. R. & Grinnell, B. W. Enhanced protein C activation and inhibition of fibrinogen cleavage by a thrombin modulator. *Science* **273**, 1389-1391, (1996).
- 7 Xu, X., Chen, Z., Wang, Y., Bonewald, L. & Steffensen, B. Inhibition of MMP-2 gelatinolysis by targeting exodomain-substrate interactions. *Biochem J* **406**, 147-155, (2007).
- 8 Lauer-Fields, J. L. *et al.* Selective modulation of matrix metalloproteinase 9 (MMP-9) functions via exosite inhibition. *J Biol Chem* **283**, 20087-20095, (2008).
- 9 Hendriks, B. S., Seidl, K. M. & Chabot, J. R. Two additive mechanisms impair the differentiation of 'substrate-selective' p38 inhibitors from classical p38 inhibitors in vitro. *BMC Syst Biol* **4**, 23, (2010).
- 10 Shah, N. G. *et al.* Novel Noncatalytic Substrate-Selective p38alpha-Specific MAPK Inhibitors with Endothelial-Stabilizing and Anti-Inflammatory Activity. *J Immunol* **198**, 3296-3306, (2017).
- 11 Panwar, P. *et al.* Tanshinones that selectively block the collagenase activity of cathepsin K provide a novel class of ectosteric antiresorptive agents for bone. *British journal of pharmacology* **175**, 902-923, (2018).
- 12 Novinec, M., Rebernik, M. & Lenarcic, B. An allosteric site enables fine-tuning of cathepsin K by diverse effectors. *FEBS letters* **590**, 4507-4518, (2016).

- 13 Duggan, K. C. *et al.* (R)-Profens are substrate-selective inhibitors of endocannabinoid oxygenation by COX-2. *Nat Chem Biol* **7**, 803-809, (2011).
- 14 Zhao, B. *et al.* Identification of gamma-secretase inhibitor potency determinants on presenilin. *J Biol Chem* **283**, 2927-2938, (2008).
- 15 Descamps, O. *et al.* AbetaPP-selective BACE inhibitors (ASBI): novel class of therapeutic agents for alzheimer's disease. *J Alzheimers Dis* **37**, 343-355, (2013).
- 16 Espeseth, A. S. *et al.* Compounds that bind APP and inhibit Abeta processing in vitro suggest a novel approach to Alzheimer disease therapeutics. *J Biol Chem* **280**, 17792-17797, (2005).
- 17 Lowe, J. T. *et al.* Synthesis and profiling of a diverse collection of azetidine-based scaffolds for the development of CNS-focused lead-like libraries. *The Journal of organic chemistry* **77**, 7187-7211, (2012).
- 18 Maianti, J. P. *et al.* Anti-diabetic activity of insulin-degrading enzyme inhibitors mediated by multiple hormones. *Nature* **511**, 94-98, (2014).
- 19 Malito, E. *et al.* Molecular bases for the recognition of short peptide substrates and cysteine-directed modifications of human insulin-degrading enzyme. *Biochemistry* **47**, 12822-12834, (2008).
- 20 Duckworth, W. C., Bennett, R. G. & Hamel, F. G. Insulin degradation: progress and potential. *Endocr Rev* **19**, 608-624, (1998).
- 21 Farris, W., Leissring, M. A., Hemming, M. L., Chang, A. Y. & Selkoe, D. J. Alternative splicing of human insulin-degrading enzyme yields a novel isoform with a decreased ability to degrade insulin and amyloid beta-protein. *Biochemistry* **44**, 6513-6525, (2005).
- 22 Tang, W. J. Targeting Insulin-Degrading Enzyme to Treat Type 2 Diabetes Mellitus. *Trends in endocrinology and metabolism: TEM* **27**, 24-34, (2016).
- 23 Kessler, J. H. *et al.* Antigen processing by nardilysin and thimet oligopeptidase generates cytotoxic T cell epitopes. *Nat Immunol* **12**, 45-53, (2011).
- 24 Chow, K. M. *et al.* Nardilysin cleaves peptides at monobasic sites. *Biochemistry* **42**, 2239-2244, (2003).
- 25 Ma, Z., Chow, K. M., Csuhai, E. & Hersh, L. B. The use of proteolysis to study the structure of nardilysin. *Archives of biochemistry and biophysics* **401**, 198-204, (2002).
- 26 Chow, K. M. *et al.* Studies on the subsite specificity of rat nardilysin (N-arginine dibasic convertase). *J Biol Chem* **275**, 19545-19551, (2000).

- 27 Leissring, M. A. *et al.* Designed inhibitors of insulin-degrading enzyme regulate the catabolism and activity of insulin. *PLoS One* **5**, e10504, (2010).
- 28 APEX2 v. 2014.11-0 (Bruker AXS, Madison, Wisconsin, USA, 2014).
- 29 Sheldrick, G. M. SHELXT - Integrated space-group and crystal-structure determination. *Acta crystallographica. Section A, Foundations and advances* **71**, 3-8, (2015).
- 30 Sheldrick, G. M. Crystal structure refinement with SHELXL. *Acta Crystallographica Section C Structural Chemistry* **71**, 3-8, (2015).
- 31 Hall, M. D. *et al.* Fluorescence polarization assays in high-throughput screening and drug discovery: a review. *Methods Appl Fluoresc* **4**, 022001, (2016).
- 32 Shen, Y., Joachimiak, A., Rosner, M. R. & Tang, W. J. Structures of human insulin-degrading enzyme reveal a new substrate recognition mechanism. *Nature* **443**, 870-874, (2006).
- 33 McCord, L. A. *et al.* Conformational states and recognition of amyloidogenic peptides of human insulin-degrading enzyme. *Proc Natl Acad Sci U S A* **110**, 13827-13832, (2013).
- 34 Rose, K. *et al.* Insulin proteinase liberates from glucagon a fragment known to have enhanced activity against Ca<sup>2+</sup> + Mg<sup>2+</sup>-dependent ATPase. *Biochem J* **256**, 847-851, (1988).